MATERIALS CHARACTERIZATION 61 (2010) 1135–1146

available at www.sciencedirect.com

ScienceDirect

www.elsevier.com/locate/matchar

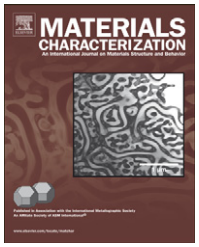

# A study of the composition and microstructure of nanodispersed Cu–Ni alloys obtained by different routes from copper and nickel oxides

*María de los A. Cangiano, Manuel W. Ojeda*, Alejo C. Carreras, Jorge A. González, María del C. Ruiz*

*Instituto de Investigaciones en Tecnología Química (INTEQUI), Universidad Nacional de San Luis-CONICET, Chacabuco y Pedernera, 5700 San Luis, Argentina*

ARTICLE DATA

*Article history:*
Received 12 April 2010
Received in revised form 9 July 2010
Accepted 19 July 2010

*Keywords:*
Cu–Ni alloy
Nanostructure
Chemical synthesis
Mechanical mixture

ABSTRACT

Mixtures of CuO and NiO were prepared by two different techniques, and then the oxides were reduced with $H_2$. *Method A* involved the preparation of mechanical mixtures of CuO and NiO using different milling and pelletizing processes. *Method B* involved the chemical synthesis of the mixture of CuO and NiO. The route used to prepare the copper and nickel oxide mixture was found to have great influence on the characteristics of bimetallic Cu–Ni particles obtained. Observations performed using the X-ray diffraction (XRD) technique showed that although both methods led to the Cu–Ni solid solution, the diffractogram of the alloy obtained with *method A* revealed the presence of NiO together with the alloy. The temperature-programmed reduction (TPR) experiments indicated that the alloy is formed at lower temperatures when using *method B*. The scanning electron microscopy (SEM) studies revealed notable differences in the morphology and size distribution of the bimetallic particles synthesized by different routes. The results of the electron probe microanalysis (EPMA) studies evidenced the existence of a small amount of oxygen in both cases and demonstrated that the alloy synthesized using *method B* presented a homogeneous composition with a Cu–Ni ratio close to 1:1. On the contrary, the alloy obtained using *method A* was not homogeneous in all the volume of the solid. The homogeneity depended on the mechanical treatment undergone by the mixture of the oxides.



## 1. Introduction

Cu–Ni alloys are widely used in different industries due to their special mechanical and chemical properties. They are highly resistant to corrosion in different media (acid, alkaline, oxidizing and reducing), present excellent electrical and thermal conductivities and are easily manufactured. For these reasons, they are widely applied in the building of ships, pipes and other seawater-related structures as well as in the building of equipments for chemical processes, heat exchangers, pumps, valves, etc. [1–3].

Besides, the giant magnetoresistance (GMR) effect shown by multilayer structures of Cu and Ni makes them useful for the manufacture of sensors for recording magnetic data and for monitoring the position of the machines' components [4]. In addition, electrochemically and thermally prepared coatings of Cu–Ni alloys are characterized by high solar absorbance and low thermal emittance; thus, resulting useful in the

* *Corresponding author*. Tel./fax: +54 2652 426711.
E-mail address: mojeda@unsl.edu.ar (M.W. Ojeda).

1044-5803/$ – see front matter © 2010 Elsevier Inc. All rights reserved.
doi:10.1016/j.matchar.2010.07.006

conversion of solar energy as a source of renewable energy [5]. Seeds of Cu–Ni alloys are also used in hyperthermia applications for tumour treatments [6].

Cu–Ni alloys are solid solutions formed by substitution. Both metals have the same crystalline structure, similar ionic radius and electronegativity and identical valence; thus, fulfilling the Hume–Rothery rules for substitution solid solutions [7].

The most widely used techniques for the synthesis of Cu–Ni alloy include electrochemical procedures [1,8–11], reduction processes in liquid phase [6,12–15], mixture of both oxides followed by reduction in gaseous phase [3], and physical methods, such as copper and nickel fusion and powder metallurgy followed by sintering [16–19].

The decrease of the grain size of a solid, down to nanometre scale, causes notable changes in its physical and chemical properties, known as "size effect". Nanoparticles show special characteristics related to thermal, electrical, magnetic, optical, mechanical and morphological-structural properties [20]. These properties mainly depend on size distribution, shape and chemical composition of the constituting grains. Obtaining nanostructures with the desired characteristics has become a subject of great scientific interest due to their potential technological and industrial applications. The development of methodologies for the synthesis of nanocrystalline alloys requires a strict control of the experimental conditions and of their correlation with the structural characteristics and with the physicochemical properties of the final product [8,21–26].

Metal fusion and mechanical mixture by milling are traditional physical methods used for the synthesis of metal alloys. The first method presents some limitations related to the thick granulometry of the product and to the high temperature required for metal fusion. On the other hand, the dry milling method does not contaminate the obtained product with solvent.

Inert gas condensation (IGC) [27,28] and mechanical milling [29] are the oldest processes used for the preparation of metals and nanostructured alloys, but they present several drawbacks. The material obtained by IGC exhibits great porosity, the production is small, and the equipment costs are high. The mechanical milling process results in the production of amorphous metals and tends to generate nanostructured materials with reticular distortions and high content of impurities [30].

The chemical processes for the synthesis of nanostructured materials offer some advantages in comparison with the physical methods in relation to simplicity, energy saving and product homogeneity. The citrate-gel method has been used for the preparation of mixed nanocrystalline oxides with specific properties, such as controlled stoichiometry and narrow particle size distribution. The low cost, simplicity and short time of production and the purity and homogeneity of the final product are included among its advantages. In addition, the speed and low temperature of the synthesis process prevent the sintering of the obtained powder; thus, it presents a large superficial area and a good sinterability in relation to powders obtained by other synthesis techniques [31–37].

The characterization of the physicochemical properties of nanostructured materials is usually carried out using several techniques [20,38,39]. X-ray diffraction (XRD), scanning electron microscopy (SEM), transmission electron microscopy (TEM) and electron probe microanalysis (EPMA) are the most widely used techniques for the structural characterization of nanomaterials because they are complementary for the crystallographic, morphological and chemical analysis of the grains constituting such structures. Scanning tunnelling microscopy (STM) and atomic force microscopy (AFM) are very useful tools for observing superficial features at nanometre scale. Differential thermal analysis (DTA), thermogravimetry (TG) analysis and temperature-programmed reduction (TPR) are generally used to study the kinetics and mechanisms of reactions and phase transformations involved in the materials synthesis processes.

In this work, a comparative study of the morphological, structural and chemical properties of Cu–Ni alloys synthesized by two different routes was performed. The synthesis methods involved the reduction of the mixture of CuO and NiO obtained by a mechanical process and by a chemical procedure. Morphological and crystallographic features of the samples were studied by means of SEM and XRD. The chemical composition and homogeneity were determined by EPMA. TPR experiments were carried out with the purpose of studying the reducibility of the involved oxides.

## 2. Experimental Procedures

### 2.1. *Reagents*

The reagents used were copper oxide (II) Mallinckrodt; nickel oxide (II) Carlo Erba; nickel nitrate (II) ($Ni(NO_3)_2.6H_2O$), Fluka; copper nitrate (II) ($Cu(NO_3)_2.2.5H_2O$), Rieldel-de Haën; and citric acid, Anedra. All the solid reagents were p.a. quality. The gases used in the different assays were 99.999% pure nitrogen, a mixture of $H_2$ (5%) in $N_2$ and a mixture of $O_2$ (10%) in $N_2$.

### 2.2. *Preparation of Mixtures of CuO and NiO*

#### 2.2.1. *Mechanical Method (Method A)*

(i) A manual mixture of powdered CuO and NiO at 50% p/p was carried out, in a Fritsch disk mill, without milling elements (sample A1).
(ii) Sample A1 was divided into several fractions, one of which was pelletized at a 300-kg/cm$^2$ pressure (sample A2).
(iii) Other fractions were subjected to milling processes of 4, 8 and 12 min, in the previously mentioned mill (samples A3, A4 and A5, respectively).
(iv) Finally, a fraction of sample A5 was manually ground in a porcelain mortar for almost 20 min (sample A6).

#### 2.2.2. *Chemical Method (Method B)*

(i) Precursor preparation: copper nitrate (II) and nickel nitrate (II) were separately dissolved in water. Then, an aqueous solution of citric acid was added to the Cu(II) and Ni(II) solution. The resulting solution was heated to 50 °C in a magnetic stirrer. After that, the solution was boiled using a heater mantle. The solvent was then removed at 75 °C under vacuum conditions using a Büchi 461 vacuum rota-vapour until a viscous gel was

obtained. The dehydration was completed by gradual heating in a vacuum heater until 100 °C, keeping this temperature for 15 hours.

(ii) Decomposition: the precursor decomposition was carried out under non isothermal conditions with a heating program of 1 °C/min, from room temperature to 280 °C, in a $N_2$ flow of 100 ml/min, keeping this temperature for 1 hour and 45 min.

(iii) Calcination: the calcination was also carried out under non isothermal conditions in an $O_2$ (10%) in a $N_2$ flow with the same heating rate of the previous stage.

### 2.3. *Reduction of the CuO and NiO Mixtures*

A quartz-made tubular reactor heated by an electric furnace was used for this procedure. Gases were purified using traps to retain water and oxygen, and the samples to be reduced were placed in a quartz crucible.

The reduction of the mixture obtained by *method A* was carried out under non isothermal conditions using a heating program of 5 °C/min, from room temperature to 450 °C, in $H_2$ (5%) in a $N_2$ (v/v) flow of 100 ml/min. The system was kept at this temperature for 30 min, and finally it was cooled in a $N_2$ gas flow. The samples obtained at this stage were identified as A1R to A6R, according to the previously performed mechanical treatment. The oxide mixture obtained by *method B* was reduced following the previously described procedure, but with a final temperature of 300 °C (sample B1R).

Figs. 1 and 2 show the flow diagrams of both synthesis routes.

### 2.4. *Temperature-Programmed Reduction Tests*

TPR experiments were carried out on samples A1, A4 and B1 using a conventional equipment and following the technique described by Barroso et al. [40]. The assays were performed with a mixture of $H_2$ (5%) in $N_2$ (v/v) and a 100-ml/min flow, by heating from 25 °C until reaching 500 °C, at a 5 °C/min rate, and keeping the sample at this temperature for 1 h.

### 2.5. *Samples Characterization*

The crystalline structure and the one direction minimum size of the phase crystallite of the solids obtained at the different stages were studied using XRD, in a Rigaku D-Max IIIC diffractometer, operated at 30 kV and 20 mA, with Cu-Kα radiation ($\lambda$=0.15418 nm), with Ni filter, and scanning an angular interval of 2$\theta$ between 10° and 70°, at a 3°/min rate. The morphological and chemical analyses were performed using SEM and EPMA. A LEO 1450VP scanning electron microscope, with an EDAX Genesis 2000 energy dispersive

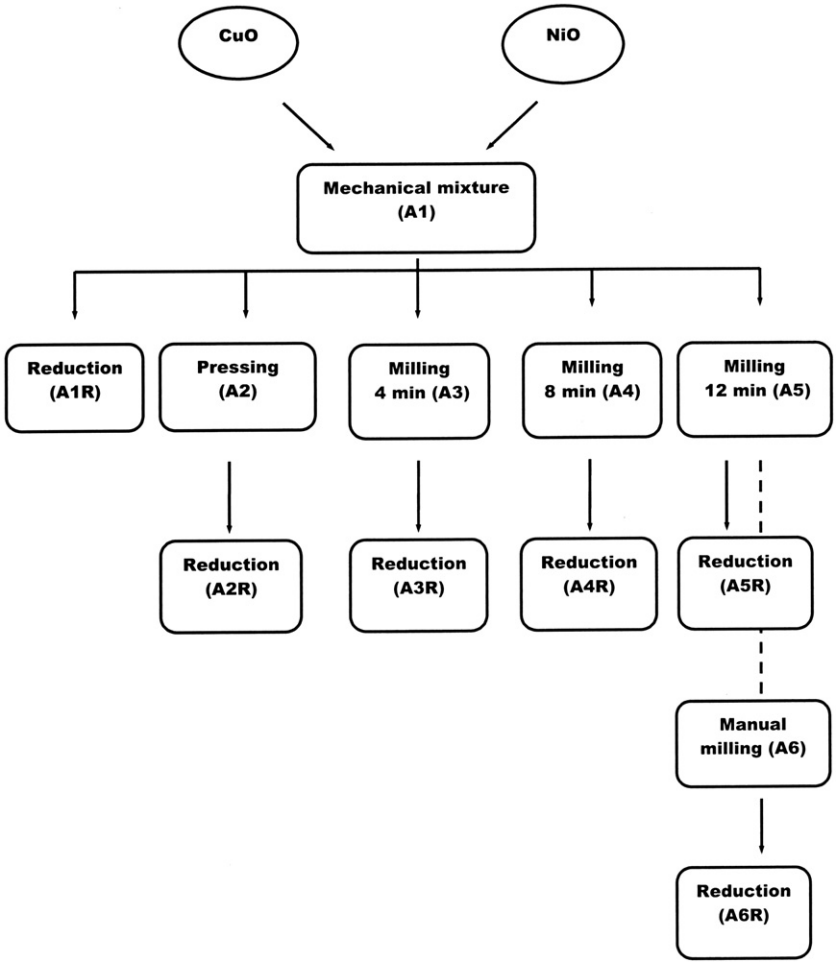


**Fig. 1 – Flow diagram for Cu–Ni alloy synthesis using *method A*.**

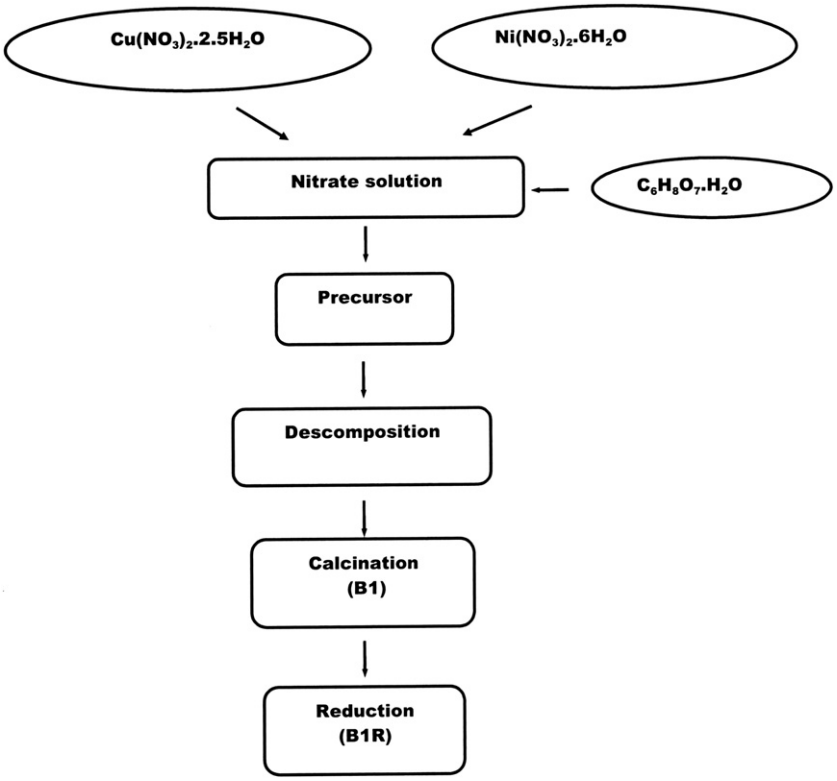


**Fig. 2 – Flow diagram for Cu–Ni alloy synthesis using *method B*.**

spectrometer (EDS), and a JEOL 6330F field emission gun-scanning electron microscope (FEG-SEM) were also used. Secondary electron images were taken at different magnifications to study the morphological and topographical details of the particles present in all the samples. Then, five particles of each sample were randomly selected, and their chemical compositions were determined by processing the corresponding *K*-line spectra obtained with an incident beam of 20 keV electrons. A standardless semi-quantitative analysis was performed for this purpose.

## 3. Results and Discussion

### 3.1. *Temperature-Programmed Reduction Tests*

The experiments of TPR were performed to study the effect of the mixture synthesis methods on the reduction temperature of the oxides synthesized mixtures and to obtain information about the feasibility of the Cu–Ni solid solution.

The results of the TPR tests are shown in Fig. 3. Curves (a) and (b) show that the reduction of pure NiO and CuO takes place around 400 °C and 350 °C, respectively. Curve (c) shows two peaks corresponding to the reduction of CuO and NiO present in the mechanical mixture (sample A1). It can be observed that both peaks appear at a lower temperature in relation to the position of each separately reduced pure oxide. The analysis of curve (d), corresponding to sample A4, indicates that the milling process produces a greater decrease of the reduction temperature. Curve (e), corresponding to the reduction of the solid obtained after the calcination stage of *method B* (sample B1), presents only one peak at approximately 250 °C.

The TPR profiles shown in Fig. 3 indicate, on the one hand, that the mixing process of CuO and NiO favours their reduction to the metallic state, and on the other hand, that the mixture obtained by the citrate-gel method is reduced at a lower temperature than the one obtained by the mechanical method.

The behaviour of the mixture of CuO and NiO in the reduction process is attributed in the case of *method* A, to a

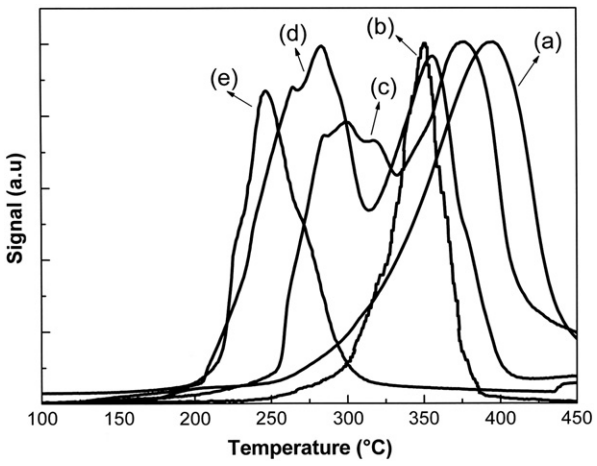


**Fig. 3 – Results of the TPR analysis. (a) Pure NiO; (b) pure CuO; (c) A1; (d) A4; and (e) B1.**

decrease in the particle size and to an increase in the homogeneity, caused by the joint milling of the oxides. Regarding *method B*, the phenomenon observed during the reduction stage is clearly favoured in relation to *method A* due to the oxide mixture present a smaller granulometry and a greater chemical homogeneity, as explained later when describing the EPMA results. This behaviour has also been found by Fierro et al. [41] who observed that, under certain experimental conditions, a decrease in the particle size and an increase of the specific surface of the CuO cause a decrease in the reduction temperature. This decrease, when working with the oxide mixture, is attributed to the formation of the Cu–Ni solid solution. It was observed that a greater formation of the solid solution was obtained when the particles of both oxides were closer, with the subsequent greater decrease of the reduction temperature. These results suggested a thermodynamic stability of the fcc cubic solid solution in relation to its equivalent pure phases. Theoretical thermodynamic calculations carried out by Yamín et al. [42] supported this hypothesis. These authors carried out ab initios calculations of molecular orbitals using the Gaussian 98 system, by means of the Density Functional Theory method (DFT) with the hybrid functionals B3LYP, using basic sets of pseudopotentials LANL2DZ.

For the theoretical calculation of the enthalpy differences between the solid solution 1:1 and its pure phases, the following fcc structures were simulated: Cu with 14 atoms using a cell parameter of 3,615 Å; Ni with 14 atoms using a cell parameter of 3.523 Å and a combination of seven atoms of Cu and seven atoms of Ni with an average cell parameter of 3.569 Å.

Specific calculations were performed for each structure, and the electronic energies were considered to compare the relative stability of the three systems. The reaction that was taken into account was $14\,Ni + 14\,Cu \rightarrow 2\,(Cu_7Ni_7)$. The values of electronic energies were $E_1$: −2370.0405 a.u. for Cu; $E_2$: −2746.5553 a.u. for Ni; and $E_3$: −2558.3475 a.u for $Cu_7Ni_7$. The electronic energy difference, $\Delta E = 2E_3 - (E_1 + E_2)$, was −0.09914 a.u., corresponding to −62.2 kcal/mol, and indicated a greater thermodynamic stability of the fcc Cu–Ni solid solution by substitution, respect to pure copper and nickel.

### 3.2. *Crystallographic Analysis*

Fig. 4 shows the X-ray diffractograms of the solids obtained at different stages of *method A*.

Fig. 4(a) shows the diffractogram of the mechanical CuO and NiO mixture (sample A1). The peaks of this diagram match with those in files JCPDS 5-661 and 4-835, corresponding to CuO and NiO, respectively.

Fig. 4(b) to (g) shows the diffractograms of samples A1R to A6R, respectively. Fig. 4(b) indicates that the reduction process of the mechanical mixture of the oxides leads to the formation of Cu and Ni in metallic state. Peaks corresponding to planes (111) around $2\theta = 44°$ and peaks corresponding to planes (200) around $2\theta = 52°$ for both metals can be clearly observed. These peaks coincide with those in files JCPDS 4-836 and 4-850, which correspond to Cu and Ni fcc in metallic state, respectively. These results demonstrate that the Cu–Ni solid solution was not formed, and each oxide was reduced to its metallic state. The one direction minimum size of the phase crystallite of sample A1R, determined by the Scherrer method, was around 40 nm.

Fig. 4(c) indicates that the pelletizing process of the oxide mixture favours metal alloy during the reduction step, as evidenced by a slight shift in the position of the metallic Ni peaks and a variation of their intensities (in relation to Cu peaks), which may be attributed to an incipient formation of the Cu–Ni solid solution. NiO peaks can also be observed at $2\theta = 37.25°$ and $2\theta = 62.89°$, which might indicate the presence of unreduced oxide.

Fig. 4(d) to (g) indicates that the milling process exerts a significant effect on the reduction of the oxide mixture since the (111) and (200) peaks, corresponding to the metallic Ni phase, have clearly shifted to lower $2\theta$ values. The position shift of the metallic Ni peaks is more evident than that of the Cu ones. The analysis of the Cu (111) peak in the ground samples is difficult because it overlaps the principal NiO peak. However, it can be observed from the Cu (200) peaks that the shift is small and their relative intensities decrease with milling. These results suggest the formation of the Cu–Ni solid solution by means of the diffusion of Cu through the Ni structure.

Besides, the presence of unreduced NiO is observed in all cases. This can be attributed to the formation mechanism of the Cu–Ni solid solution, which will be discussed later.

The positions of the Ni (111) and (200) peaks in the diffractograms of samples A1R to A6R were determined by Lorentzian fit. Fig. 5 shows the results of the adjustment obtained for the (111) peak; identical correlation was found for the (200) peak. The analysis of the shifts in the positions of the Ni (111) and (200) peaks indicates that in the case of the mechanical mixture reduction (sample A1R), the Cu–Ni solid solution was not formed; for the sample AR2, there exists an incipient formation of the Cu–Ni solid solution, and for samples A3R to A6R, a partial alloying of both metals occurs.

These results are in agreement with those reported by Durivault et al. [19] on the preparation of $Cu_x$–$Ni_{1-x}$ materials by mechanical milling. These authors used XRD to characterize the samples of the obtained powder and observed a progressive shift of Cu–Ni phase peaks to lower diffraction angles as the milling time increased.

The one direction minimum size of the phase crystallite for samples A2R to A6R, for which a partial formation of the solid solution was obtained, could not be estimated by this method due to the overlapping of the peak corresponding to the solid solution with the peaks of Cu and Ni as can be appreciated in Fig. 5. This overlapping did not permit the application of the Scherrer equation.

Fig. 6 shows the X-ray diffractograms of the solids obtained using *method B*. Fig. 6 (a) corresponds to the solid obtained in the calcination stage (sample B1) and is in agreement with files JCPDS 5-661 and 4-835 of CuO and NiO, respectively. These results indicate that the mixture of Cu and Ni oxides was obtained at this stage of the synthesis process. Fig. 6(b) shows the diffractogram of the sample obtained after reducing the mixture of Cu and Ni oxides (sample B1R). Only two peaks can be observed, at $2\theta = 44.002°$ and $2\theta = 51.1°$, which are intermediate positions in relation to the peaks corresponding to the pure metals.

The centers of the Ni (111) and (200) peaks, in the diffractogram of sample B1R, were determined using Lorentzian

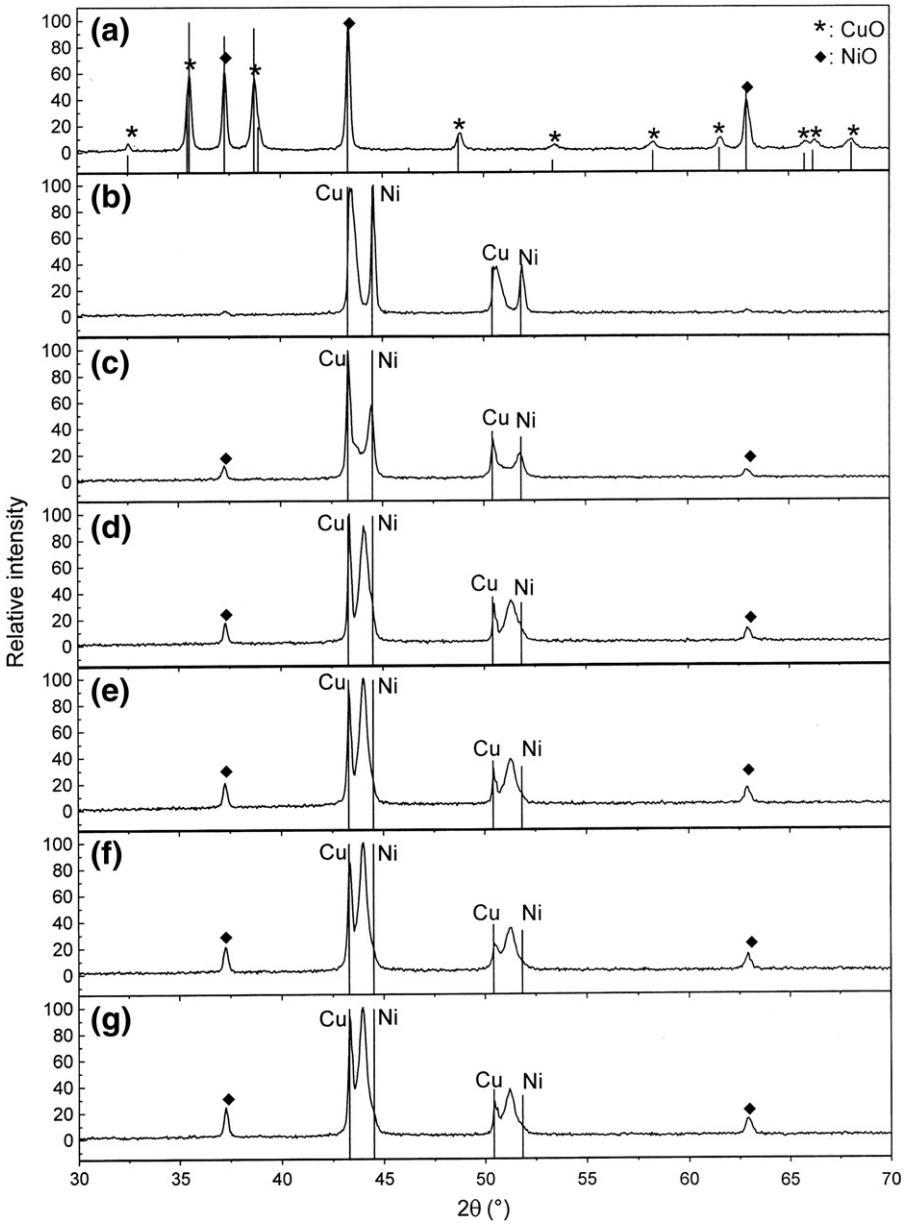


**Fig. 4 – X-ray diffractograms of the solids obtained at different stages of *method A*. (a) A1; (b) A1R; (c) A2R; (d) A3R; (e) A4R; (f) A5R; (g) A6R.**

adjustment. The result for the (111) peak is shown in the inset of Fig. 6b, where the shift of the peak position can be clearly observed. Identical correlation was found for the (200) peak. The position shift in the Ni (111) peak from $2\theta = 44.505°$ to $2\theta = 44.002°$ indicates the formation of the Cu–Ni solid solution. These results are in agreement with those reported by Rao et al. [15] and Songping et al. [43,44] in relation to the peak positions in the XRD diagram of the Cu–Ni (1:1) alloy.

The one direction minimum size of the phase crystallite of the alloy obtained by *method B* (sample B1R) was calculated using the Scherrer equation, and the value obtained was 15.45 nm. In this case, unlike the samples A2R to A6R, there was no overlapping with the Cu and Ni peaks since there appeared an only peak corresponding to the solid solution in the position $2\theta = 44.002°$; therefore, the grain size was determined without difficulties.

### 3.3. *Morphological Analysis*

Fig. 7 shows micrographs of the solids obtained at different stages of *method A*.

Fig. 7(a) corresponds to the mechanical mixture of CuO and NiO (sample A1) and shows particle agglomerates (with diameters ranging between 1 and 3 μm) and individual sphere-like particles (with diameters ranging between 0.1 and 0.5 μm).

Fig. 7(b) corresponds to the solid resulting from the reduction of the unground mixture (sample A1R), and the micrograph indicates that after reduction the morphology of the solid changed significantly. Stick-like particles (between 1 and 3 μm long and approximately 0.5 μm wide) and some sphere-like particles, with a diameter of approximately 0.5 μm, can be observed.

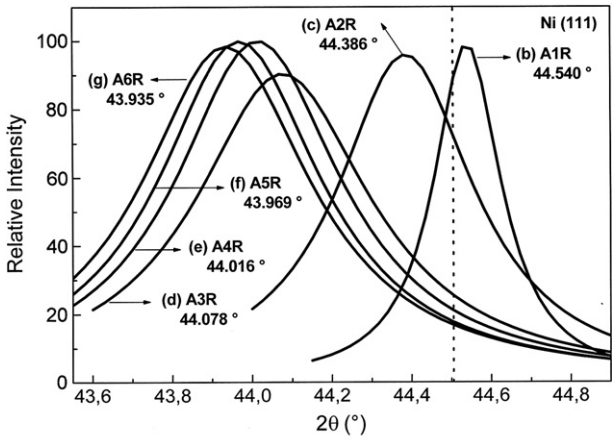


**Fig. 5 – Lorentzian adjustment of the position of the Ni (111) peak. Curves (b) to (g) correspond to samples A1R to A6R, respectively. The vertical dotted line corresponds to the position of the pure Ni (111) peak.**

Fig. 7(c) shows the solid obtained after reducing the mixture of the oxides milled during 8 min (sample A4R). This figure shows sphere-like particles with diameters ranging between 0.2 and 0.5 μm and agglomerates of irregular-shaped particles.

Fig. 7(d) and (e) show the solid obtained after reducing the mixture of the oxides milled during 12 min in a disk mill (sample A5R) and then manually ground in a porcelain mortar for almost 20 min (sample A6R). Fig. 7(d) shows particles slightly smaller than Fig. 7(c), although the appearance and the morphology of both solids are similar. This decrease in the particle size is due to the intensity and duration of the milling process of the CuO and NiO mixture. Fig. 7(e) shows agglomerates of particles ranging between 100 and 500 nm, with grains around 20 nm.

Fig. 8 shows the micrographs of the solids obtained at different stages of *method B*.

Fig. 8(a), corresponding to a typical particle of the solid obtained after the calcination stage (sample B1), shows a flat particle accompanied by smaller irregular-shaped particles. Fig. 8(b), corresponding to a representative particle of the solid obtained after the reduction process (sample B1R), shows a flat irregular-shaped particle. Fig. 8(c) and (d) also show micrographs of sample B1R, but taken at a greater magnification with an FEG-SEM. A fine granulometry can be observed in the particle surface shown in Fig. 8(c), with a grain size ranging between 14 and 23 nm, which is consistent with the one direction minimum size of the phase crystallite obtained by XRD. Fig. 8(d) shows a crack in an alloy particle where an internal morphology similar to the superficial one is observed.

The SEM characterization of the solids obtained after the reduction of the different mixtures of CuO and NiO reveals significant differences in the particles morphology and size. This clearly indicates that the method used to obtain the oxide mixtures exerts a marked influence on their characteristics and, consequently, on the features of the solid obtained after the reduction stage.

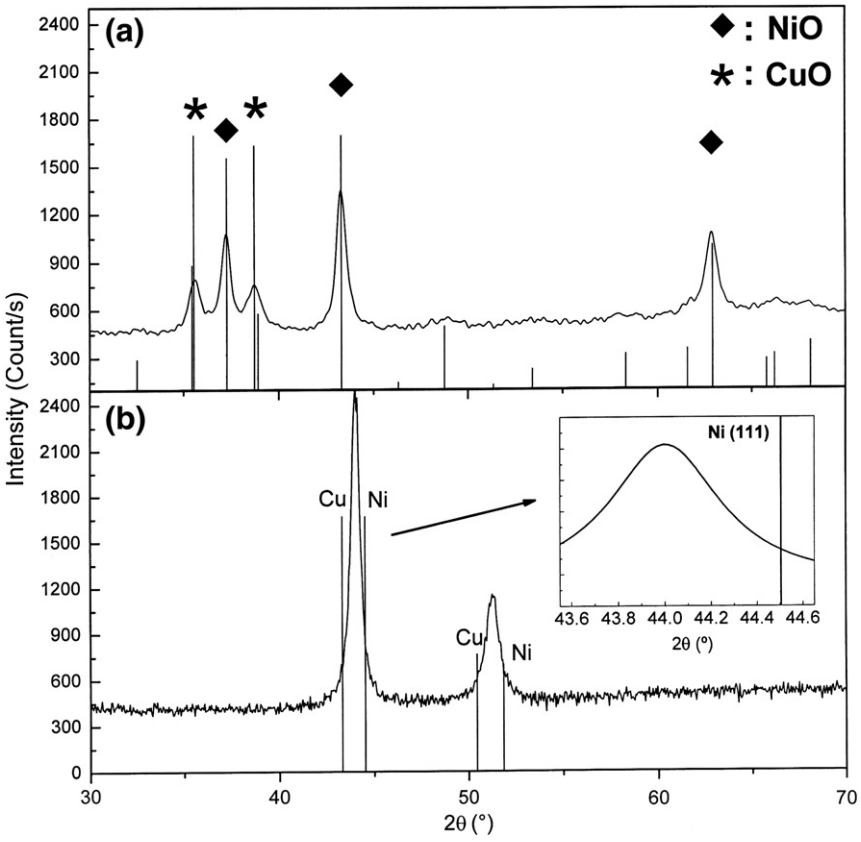


**Fig. 6 – X-ray diffractograms of the solids obtained in the calcination and reduction stages of *method B*. (a) B1; (b) B1R and inset of the Lorentzian adjustment of the Ni (111) peak (the vertical line corresponds to position (111) of pure Ni).**

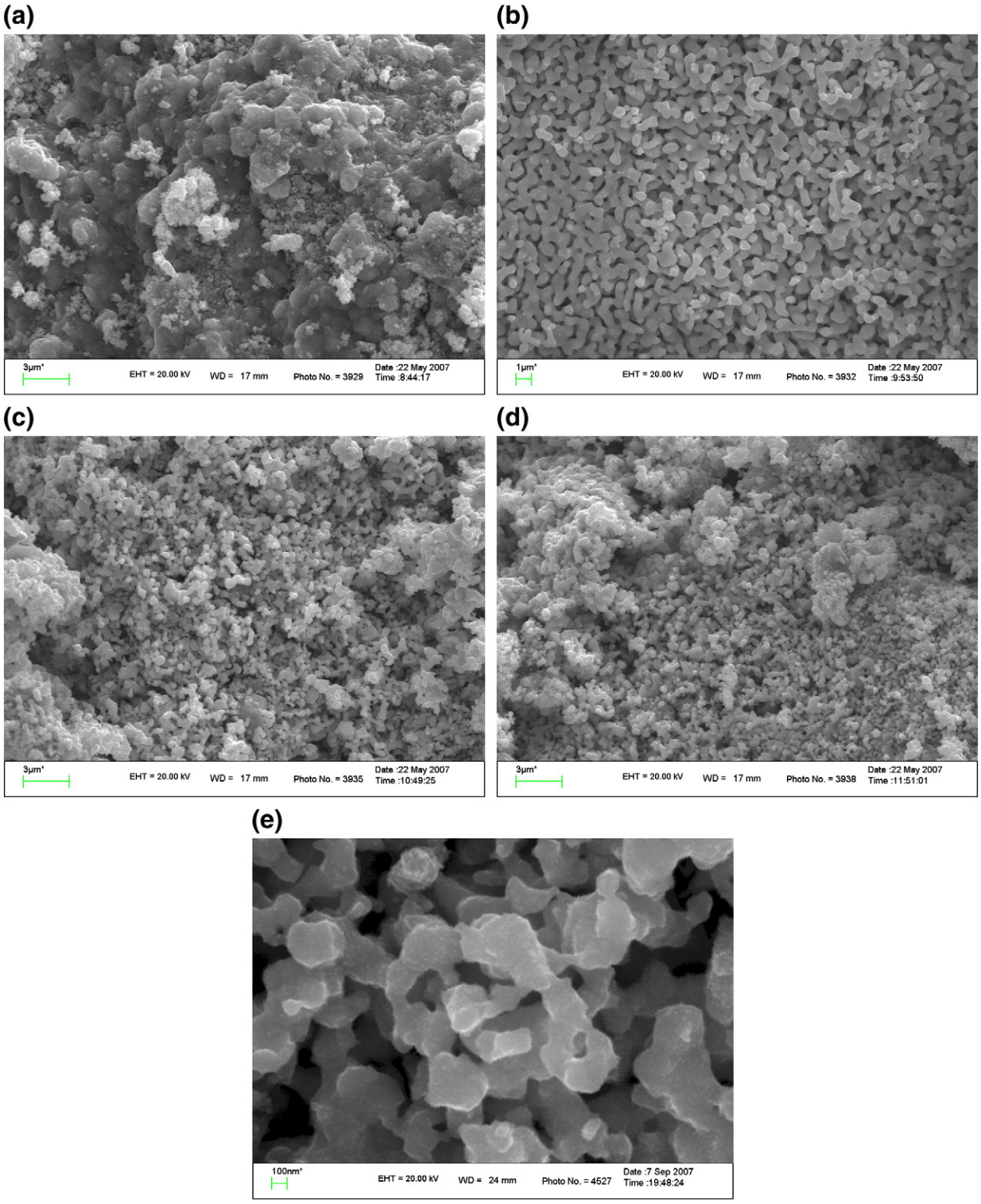


**Fig. 7 – SEM micrographs of samples obtained at different stages of *method A*. (a) A1; (b) A1R; (c) A4R; (d and e) A6R, with different magnifications.**

### 3.4. *Chemical Analysis*

Fig. 9 shows typical EDS spectra of the solids obtained at different stages of both synthesis methods. The elements detected in all the samples were O, Ni and Cu; the presence of carbon peaks is mainly due to the coating applied on the samples prior to the SEM-EPMA analysis, and the mall concentrations of Fe (less than 0.3 wt.%), detected in samples A4R and A6R, are due to the contamination from the milling equipment.

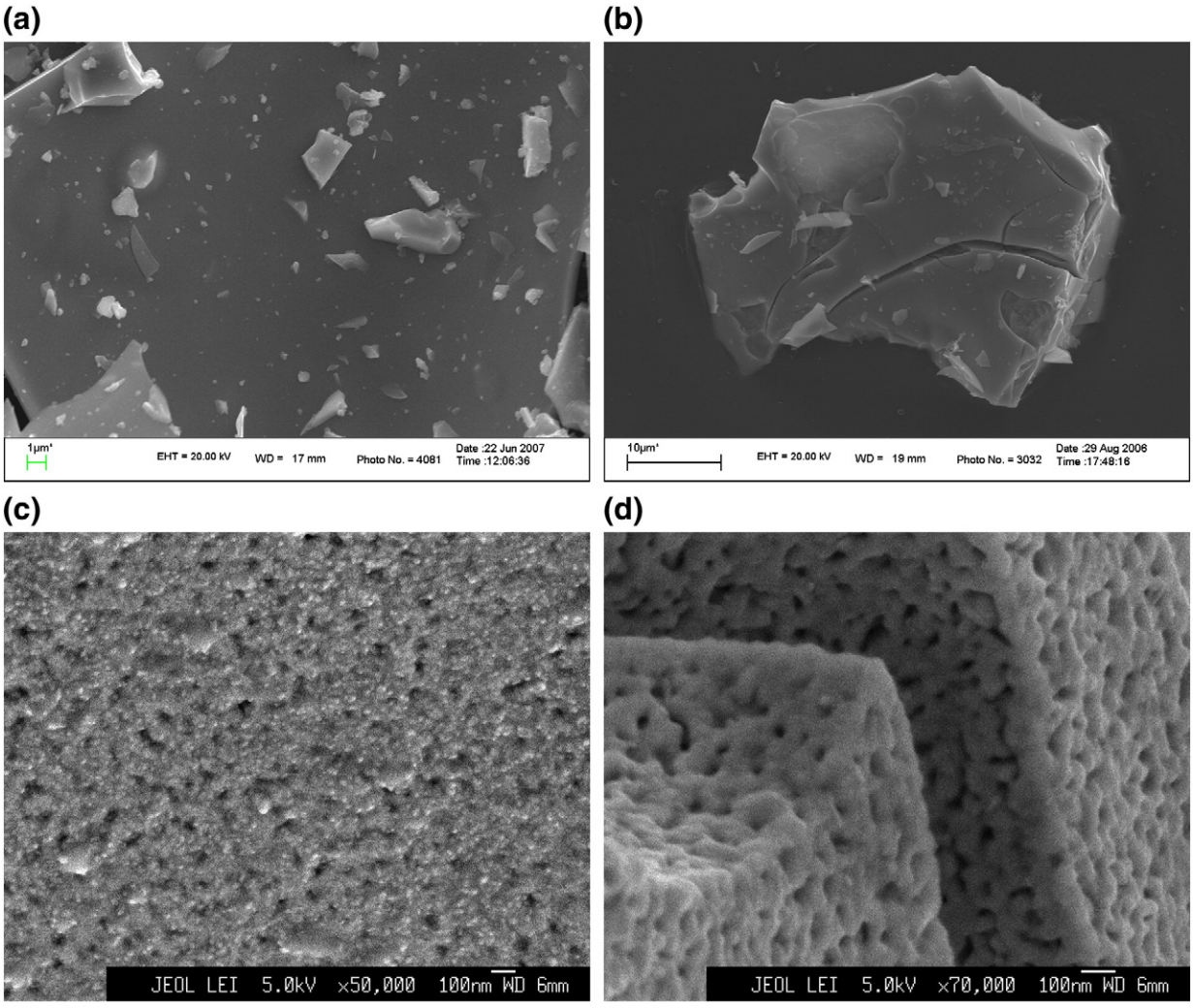


**Fig. 8 – SEM (a and b) and FEG-SEM (c and d) micrographs of samples obtained in the calcination and reduction stages of *method B*. (a) B1; (b to d) B1R, with different magnifications.**

Tables 1 and 2 present the quantification results of the solids obtained by *methods A* and *B*, respectively. The concentration data of Fe are not included in Table 1 because they are lower than the uncertainties of the quantification method.

The comparison between Tables 1 and 2 shows that the oxygen percentages detected in the CuO and NiO mixtures obtained through both methods (samples A1 and B1) are similar, and the average values are 18 and 20.6 wt.%, respectively. In the reduced samples A1R, A4R and A6R (Table 1), the oxygen concentrations range between 3 and 5 wt.%. The presence of oxygen in the alloys obtained using *method A* seems to indicate that the reduction has not been quantitative, leaving remnant oxides, as evidenced by the NiO peaks observed in the diffractograms of the reduced mechanical mixtures (Fig. 4). In the case of the alloy obtained by *method B* (sample B1R), the average oxygen concentration from Table 2 is 3.6 wt.%. The existence of oxygen in this sample can be attributed to a reoxidation of the alloy nanoparticles surface, which causes the formation of Cu and Ni amorphous oxidized species that cannot be observed by XRD. Other authors have observed similar phenomena in their investigations related to the synthesis of Ni and Cu nanoparticles. Davar et al. [45] synthesized Ni and NiO nanoparticles by a chemical route, and, using X-ray photoelectron spectroscopy (XPS) and Fourier transform infrared (FT-IR) spectroscopy, they observed that, when the particle size was 14 nm, the exposition to air and environmental humidity caused the oxidation of the nickel surface. Palza et al. [46], using XPS and XRD, analyzed Cu nanoparticles synthesized by evaporation in the presence of an inert gas and identified small quantities of $Cu_2O$ on the metal surface. They attributed the presence of this oxide to the superficial oxidation of the copper caused by environmental $O_2$ when removing the powders from the evaporation equipment.

The data in Tables 1 and 2 also show that the alloy synthesized by *method B* has a Cu/Ni ratio close to 1 and exhibits a better chemical homogeneity than that obtained by *method A*, as can be observed from the average and dispersions of the quantitative values.

The agreement in the results of the characterizations carried out using XRD and EPMA shows that the synthesis of

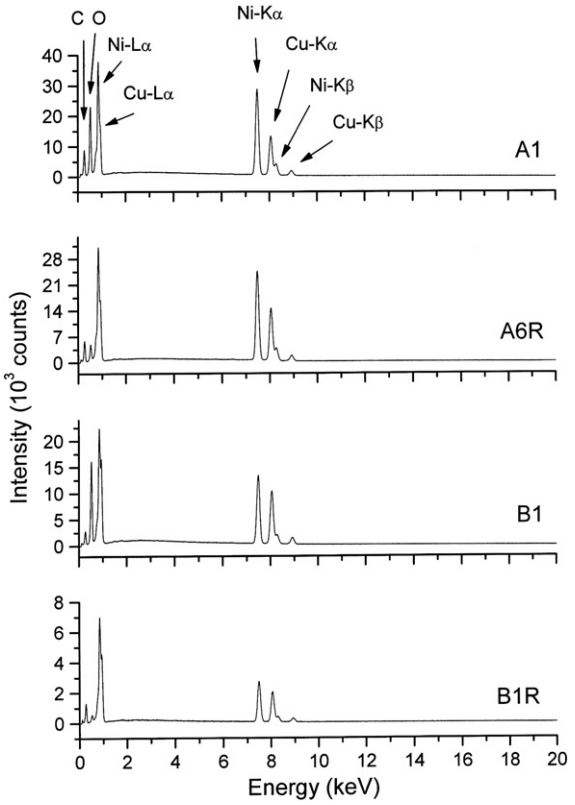


**Fig. 9 – Typical EDS spectra of samples A1, A6R, B1 and B1R.**

the oxide mixture by the citrate-gel chemical route (*method B*) permits to obtain a homogeneous nanoalloy of Cu–Ni (1:1) in the reduction stage.

### 3.5. *Mechanism of Alloy Formation*

The results from the analyses suggest that the characteristics of the alloys obtained by both studied methods depend on the mechanism by which the Cu–Ni solid solution is formed. For this reason, reduction assays of CuO, NiO and the mixture of both were carried out separately in order to investigate the mechanism leading to the formation of the Cu–Ni alloy. When the CuO reduction was finished, it was observed that the quartz crucible, where the sample was placed, was completely covered by a fine layer of metallic Cu, which indicated the Cu° sublimation and its later deposition on the crucible. Fierro et al. [41] observed similar behaviours in their TPR studies of

**Table 2 – *Method B*. Composition of 5 particles of each sample analyzed by SEM (% in weight), obtained using EDS.**

| Sample | B1 | | | B1R | | |
|---|---|---|---|---|---|---|
| Element | O | Ni | Cu | O | Ni | Cu |
| wt.% | 24 | 38 | 38 | 3 | 48 | 49 |
| | 23 | 37 | 40 | 5 | 48 | 47 |
| | 27 | 36 | 37 | 4 | 49 | 47 |
| | 10 | 45 | 45 | 2 | 48 | 50 |
| | 19 | 39 | 42 | 4 | 48 | 48 |
| Average | 20.6 | 39.0 | 40.4 | 3.6 | 48.2 | 48.2 |
| Dispersion | 6.6 | 3.5 | 3.2 | 1.1 | 0.4 | 1.3 |

CuO. No similar phenomenon was observed in the reduction of NiO and of the mixture.

These observations related to the Cu° sublimation, together with the results of the XRD and EPMA characterizations and the "ab initio" calculations (Section 3.1), permit to propose the following reaction mechanism for the formation of the Cu–Ni alloy:

Stage 1

$$CuO + H_2 \rightarrow Cu^{\circ} + H_2O$$

Stage 2

$$2Cu^{\circ} + NiO \rightarrow CuO + Cu\text{–}Ni$$

The CuO formed in stage 2 is again reduced by $H_2$ according to stage 1; the Cu° diffuses towards the unreduced NiO and is incorporated to the Ni lattice to form the Cu–Ni (1:1) alloy, which is thermodynamically favourable, according to the value of the calculated electronic energy change (−62.2 kcal/mol).

This mechanism permits to explain the presence of unreduced NiO in the alloy obtained by *method A*. Cu° deposition on the surface of the unreduced mixture of oxides may hinder the transference of the gaseous reagent towards the surface of the solid, which might interfere with stage 1 and consequently stage 2. Besides, the fact that the mixture of the oxides is not completely homogeneous also hinders the diffusion of Cu°, formed in stage 1, towards the unreduced NiO, partially inhibiting the formation of the Cu–Ni (1:1) solid solution.

The differences in composition and crystalline structure observed in the alloys obtained by each method may be explained by the proposed mechanism. In *method B* (unlike *method A*), stages 1 and 2 occur without important difficulties

**Table 1 – *Method A*. Composition of 5 particles of each sample analyzed by SEM (% in weight), obtained using EDS.**

| Sample | A1 | | | A1R | | | A4R | | | A6R | | |
|---|---|---|---|---|---|---|---|---|---|---|---|---|
| Element | O | Ni | Cu | O | Ni | Cu | O | Ni | Cu | O | Ni | Cu |
| wt.% | 21 | 77 | 2 | 3 | 87 | 10 | 4 | 60 | 36 | 4 | 50 | 46 |
| | 16 | 68 | 16 | 6 | 43 | 51 | 4 | 59 | 36 | 6 | 49 | 45 |
| | 17 | 75 | 8 | 2 | 85 | 13 | 5 | 56 | 37 | 7 | 54 | 39 |
| | 14 | 48 | 38 | 2 | 92 | 6 | 6 | 62 | 31 | 3 | 60 | 37 |
| | 22 | 23 | 55 | 2 | 91 | 7 | 6 | 66 | 27 | 5 | 57 | 38 |
| Average | 18.0 | 58.2 | 23.8 | 3.0 | 79.6 | 17.4 | 5.0 | 60.6 | 33.4 | 5.0 | 54.0 | 41.0 |
| Dispersion | 3.4 | 22.8 | 22.1 | 1.7 | 20.7 | 19.0 | 1.0 | 3.7 | 4.3 | 1.6 | 4.6 | 4.2 |

since the composition of the oxide mixture is practically homogeneous. Therefore, stage 2 is very fast and the Cu° is not deposited on the surface of the solid before reacting; thus, stage 1 is not affected by a resistance to the mass transference from $H_2$ to the surface of the oxides.

## 4. Conclusions

The way used to prepare the CuO and NiO mixtures exerts a notable influence on the physicochemical characteristics of the products obtained after the reduction stage. The reduction of the oxide mixtures prepared by a mechanical process of milling and pelletizing of the pure oxides (*method A*) and by a chemical synthesis using the citrate-gel technique (*method B*) led to the production of solids with different morphological, structural and compositional characteristics.

Spherical particles and agglomerates of irregular-shaped particles, whose dimensions decreased with the milling time, were obtained using *method A*. The solid synthesized using *method B* exhibited flat and smooth particles, with a homogeneous and nanometric grain structure.

The XRD studies showed the NiO structure together with the alloy obtained by *method A*. In relation to the alloy synthesized by *method B*, the peaks corresponding to the crystalline structures of CuO and NiO were not observed in the diffractogram.

The reduction process of the oxide mixture prepared by *method A*, depending on the type of the mechanical treatment, led to obtain a Cu and Ni mixture with a particle of 40 nm or to the partial formation of the Cu–Ni solid solution, with an heterogeneous Cu/Ni ratio among the different particles, which size was 20 nm.

When the oxide mixture synthesized by method B was reduced, the Cu–Ni alloy was obtained completely with a Cu/Ni ratio very close to 1, a great chemical homogeneity and a particle size of approximately 15 nm.

## Acknowledgments

The authors wish to thank the Universidad Nacional de San Luis, Consejo Nacional de Investigaciones Científicas y Técnicas (CONICET) and Fondo para la Investigación Científica y Técnológica (FONCyT), Argentina, for the financial support.

SEM and EPMA analyses were carried out using equipments from the Laboratorio de Microscopia Electrónica y Microanálisis (LABMEM) of the Universidad Nacional de San Luis, Argentina, and from the Electron Microscopy Laboratory of the Brazilian Synchrotron Light Laboratory (LNLS), Campinas-SP, Brazil.

## REFERENCES

[1] Ghosh SK, Grover AK, Dey GK, Totlani MK. Nanocrystalline Ni–Cu alloy plating by pulse electrolysis. Surf Coat Technol 2000;126:48–63.
[2] Shams El Din AM, El Dahshan ME. Dissolution of copper and copper–nickel alloys in aerated dilute HCl solutions. Desalination 2000;130:89–97.
[3] Jena PK, Brocchi EA, Motta MS. Preparation of Cu–Ni alloys through a new chemical route. Metall Mater Trans B 2004;35B: 1107–12.
[4] Ebrahimi F, Kong D. Effect of microstructure on strength and fracture of electrodeposited Cu/Ni layered nano-composites. Scripta Mater 1999;40:609–16.
[5] Aravinda CL, Bera P, Jayaram V, Sharma AK, Mayanna SM. Characterization of electrochemically deposited Cu–Ni black coatings. Mater Res Bull 2002;37:397–405.
[6] Chatterjee J, Bettge M, Haik Y, Chen CJ. Synthesis and characterization of polymer encapsulated Cu–Ni magnetic nanoparticles for hyperthermia applications. J Magn Magn Mater 2005;293:303–9.
[7] Shackelford JF, Güemes A. Introducción a la Ciencia de Materiales para Ingenieros. 4ta ed. Madrid: Prentice Hall Iberia; 1998.
[8] Froes FH (Sam), Senkov ON, Baburaj EG. Synthesis of nanocrystalline materials—an overview. Mat Sci Eng A 2001;301:44–53.
[9] Kazeminezhad I, Schwarzacher W. Magnetic properties of alloy films prepared by fast pulse-plating. J Magn Magn Mater 2001;226–230:1650–3.
[10] Kazeminezhad I, Schwarzacher W. Studying the transition from multilayer to alloy in the Cu–Ni system. J Magn Magn Mater 2002;240:467–8.
[11] Glibin VP, Kuznetsov BV, Vorobyova TN. Investigation of the thermodynamic properties of Cu–Ni alloys obtained by electrodeposition or by coating. J Alloys Compd 2005;386: 139–43.
[12] Li YD, Li LQ, Liao HW, Wang HR. Preparation of pure nickel, cobalt, nickel–cobalt and nickel–copper–alloys by hydrothermal reduction. J Mater Chem 1999;9:2675–7.
[13] Bonet F, Grugeon S, Dupont L, Herrera Urbina R, Guéry C, Tarascon JM. Synthesis and characterization of bimetallic Ni–Cu particles. J Solid State Chem 2003;172:111–5.
[14] Niu HL, Chen QW, Lin YS, Jia YS, Zhu HF, Ning M. Hydrothermal formation of magnetic Ni–Cu alloys nanocrystallites at low temperatures. Nanotech 2004;15:1054–8.
[15] Rao GR, Mishra BG, Sahu HR. Synthesis of CuO, Cu and CuNi alloys particles by solution combustion using carbohydrazide and *N*-tertiarybutoxy-carbonylpiperazine fuels. Mater Lett 2004;58:3523–7.
[16] Davis JR. Metals Handbook. Desk ed. Ohio: ASM Internacional; 1998.
[17] Niu Y, Gesmundo F, Farne G, Li YS, Matteazzi P, Randi G. The air oxidation of nanocrystalline Cu-10wt.%Ni alloy at 800 °C. Corrosion Sci 2000;42:1763–77.
[18] Agnew SR, Elliott BR, Youngdahl CJ, Hemker KJ, Weertman JR. Microstructure and mechanical behavior of nanocrystalline metals. Mat Sci Eng 2000;A285:391–6.
[19] Durivault L, Brylev O, Reyter D, Sarrazin M, Bélanger D, Roué L. Cu–Ni materials prepared by mechanical milling: their properties and electrocatalytic activity towards nitrate reduction in alkaline medium. J Alloys Compd 2007;432:323–32.
[20] Hosokawa M, Nogi K, Naito M, Yokoyama T. Nanoparticle Technology Handbook. The Netherlands: Elsevier; 2007.
[21] Bonfiglioli A, Mari EA, Milani P, Silva S. Nanotecnologías y materiales. In: Ibáñez LAA, editor. Argentina: Editorial Ciclo; 2002. http://www.ceramicaycristal.com.ar/c-ciencia.htm.
[22] Tjong SC, Chen H. Nanocrystalline materials and coatings. Mat Sci Eng 2004;R45:1–88.
[23] Kumar KS, Van Swygenhoven H. Mechanical behavior of nanocrystalline metals and alloys, S. Suresh. Acta Mater 2003;51:5743–74.
[24] Padmanabhan KA. Mechanical properties of nanostructured materials. Mat Sci Eng 2001;A304–306:200–5.
[25] Gonsalves KE, Li H, Perez R, Santiago P, Jose-Yacaman M. Synthesis of nanostructured metals and metal alloys from organometallics. Coord Chem Rev 2000;206–207:607–30.

[26] Schoonman J. Nanostructured materials in solid state ionics. Solid State Ionics 2000;135:5–19.
[27] Birringer R, Gleiter H. Encyclopedia of Material Science and Engineering: Supplement 1. Oxford: Pergamon Press; 1988.
[28] Gleiter H. Nanostructured materials: state of the art and perspectives. Nanostruct Mater 1995;6:3–14.
[29] Koch CC, Cho YS. Nanocrystals by high energy ball milling. Nanostruct Mater 1992;1:207–12.
[30] Dao M, Lu L, Asaro RJ, De Hosson JTM, Ma E. Toward a quantitative understanding of mechanical behavior of nanocrystalline metals. Acta Mater 2007;55:4041–65.
[31] Biamino S, Badini C. Combustion synthesis of lanthanum chromite starting from water solutions: investigation of process mechanism by DTA-TGA-MS. J Eur Ceram Soc 2004;24:3021–34.
[32] Zhang H, Jia X, Liu Z, Li C. The low temperature preparation of nanocrystalline $MgAl_2O_4$ spinel by citrate sol–gel process. Mater Lett 2004;58:1625–8.
[33] Saberi A, Golestani-Fard F, Sarpoolaky H, Willert-Porada M, Gerdes T, Simon R. Chemical synthesis of nanocrystalline magnesium aluminate spinel ($MgAl_2O_4$) via nitrate-citrate combustion. J Alloys Compd 2008;462:142–6.
[34] Vivekanandhan S, Venkateswarlu M, Satyanarayana N. Synthesis and characterization of nanocrystalline $LiNi_{0.5}$-$Co_{0.5}VO_4$ powders by citric acid assisted sol–gel combustion process. J Alloys Compd 2008;462:328–34.
[35] Wu ZJ, Zhao XB, Tu J, Cao GS, Tu JP, Zhu TJ. Synthesis of $Li_{1+x}V_3O_8$ by citrate sol–gel route at low temperature. J Alloys Compd 2007;403:345–8.
[36] Wu Y, He Y, Wu T, Chen T, Weng W, Wan H. Influence of some parameters on the synthesis of nanosized NiO material by modified sol–gel method. Mater Lett 2007;61:3174–8.
[37] Sahi S, Daud AR, Hashim M. A comparative study of nickel–zinc ferrites by sol–gel route and solid-state reaction. Mater Chem Phys 2007;106:452–6.
[38] Adams F, Van Vaeck L, Barrett R. Advanced analytical techniques: platform for nano materials science. Spectrochimica Acta B 2005;60:13–26.
[39] Redlich Ph, Carroll DL, Ajayan PM. High spatial resolution imaging and spectroscopy in nanostructures. Curr Opin Solid State Mater Sci 1999;4:325–36.
[40] Barroso MN, Gomez MF, Arrúa LA, Abello MC. Hydrogen production by ethanol reforming over NiZnAl catalysts. Appl Catal A 2006;304:116–23.
[41] Fierro G, Jacono ML, Inversi M, Porta P, Lavecchia R. A study of anomalous temperature-programmed reduction profiles of $Cu_2O$, CuO, and CuO–ZnO catalysts. J Catal 1994;148:709–21.
[42] L. Yamín, M. Cangiano, M. Santillán, J. González, Estudio de la estabilidad termodinámica de la aleación Cobre-Níquel 1:1 (Monel), in: Anales XXVI Congreso Argentino de Química, 2006.
[43] Songping W, Ping N, Li J, Zhenou Z. Preparation of ultra-fine copper–nickel bimetallic powders with hydrothermal-reduction method. Mater Chem Phys 2007;105:71–5.
[44] Songping W. Preparation of ultra fine nickel–copper bimetallic powder for BME-MLCC. Microelectron J 2007;38:41–6.
[45] Davar F, Fereshteh Z, Salavati-Niasari M. Nanoparticles Ni and NiO: synthesis, characterization and magnetic properties. J Alloys Compd 2009;476:797–801.
[46] H. Palza, M. Pilleux, J. Pennaroli, Revista electrónica ciencia abierta 21 (2003) http://cabierta.uchile.ch, ISSN 0717–8948.